

How well do forecast models represent observed long-lived Rossby wave packets during southern hemisphere summer?

Iago Pérez-Fernández  | Marcelo Barreiro 

Departamento de Ciencias de la atmósfera y Física de los Océanos, Facultad de Ciencias, Universidad de la República, Montevideo, Uruguay

Correspondence

Iago Pérez-Fernández, Departamento de Ciencias de la atmósfera y Física de los Océanos, Facultad de Ciencias, Universidad de la República, Montevideo, Uruguay.

Email: iperez@fisica.edu.uy

Funding information

H2020 Marie Skłodowska-Curie Actions, Grant/Award Number: 813844; Programa de Desarrollo de las Ciencias Básicas

Abstract

Rossby wave packets (RWPs), are atmospheric perturbations linked to the occurrence of extreme weather events such as heatwaves, extratropical cyclone development and other equally destructive phenomena. Under certain circumstances, these packets can last from several days to 2–3 weeks in the atmosphere. Therefore, forecast models should be able to correctly predict their formation and development to enhance extreme weather events prediction from 10 to 30 days in advance. In this study, we assess whether the NCEP and IAP-CAS sub-seasonal forecast models can predict the evolution of observed RWPs that last more than 8 days (long-lived RWPs or LLRWPs) during southern hemisphere summer. Results show that the NCEP (IAP-CAS) model forecasts LLRWPs that appear eastward (westward) from the observed LLRWPs. Both models forecasted LLRWPs that rapidly lose energy after the 6th–7th lead day of simulation, which could limit LLRWPs prediction to the synoptic time scale. Additionally, both models better forecast LLRWPs when the packets manifest in the eastern Pacific. Southern Annular mode (SAM) and El Niño Southern-Oscillation (ENSO) do not seem to exert a large influence in the representation of LLRWPs. Nevertheless, during the best LLRWPs forecasts, the observed circulation anomalies signal the manifestation of negative SAM events. In contrast, both forecast models struggle at forecasting LLRWPs when a blocking situation develops to the South of Australia. Lastly, an inactive Madden Julian Oscillation (MJO) seems to favor the development of accurate LLRWPs forecasts, whereas during phases 3, 5 in the NCEP model and 3, 8 for IAP-CAS, the models struggle at forecasting LLRWPs.

KEYWORDS

IAP-CAS, MJO, NCEP, Rossby wave packets, S2S

1 | INTRODUCTION

Rossby wave packets (RWPs) are upper-level atmospheric synoptic scale perturbations located in mid-latitudes that manifest as high amplitude meanderings of the jet

stream. These wave packets travel by downstream development mechanisms, transporting large quantities of energy in the process (Chang, 2000; Chang & Yu, 1999; Yeh, 1949). RWPs are related to storm track variability (Souders et al., 2014a), extratropical cyclone development

This is an open access article under the terms of the [Creative Commons Attribution](https://creativecommons.org/licenses/by/4.0/) License, which permits use, distribution and reproduction in any medium, provided the original work is properly cited.

© 2023 The Authors. *Atmospheric Science Letters* published by John Wiley & Sons Ltd on behalf of the Royal Meteorological Society.

(Chang 2005; Sagarra & Barreiro, 2020) as well as to the manifestation of extreme rainfalls and heatwaves (Chang, 2005; Grazzini & Vitart, 2015; O'Brien & Reeder, 2017; Wirth et al., 2018). Furthermore, these packets increase medium to extended range forecast uncertainty in the areas they cross (Zheng et al., 2013). Most RWPs last less than a week in the atmosphere, although under certain circumstances they can last up to 2–3 weeks before disappearing (Grazzini & Vitart, 2015). When RWPs last more than 8 days in the atmosphere, they are referred as long-lived RWPs or LLRWPs (Grazzini & Vitart, 2015; Pérez et al., 2021).

Due to their link to extreme weather events and their impact in atmospheric predictability, it is important that numerical weather prediction models have a good representation of the development of RWPs to obtain skillful forecasts (Quinting & Vitart, 2019). An accurate representation of LLRWPs development can enhance extreme weather events detection up to 10–30 days in advance.

Quinting and Vitart (2019) analyzed the representation of RWPs in various sub-seasonal to seasonal models (S2S) during northern hemisphere winter, concluding that S2S models are able to give a good estimation of the characteristics of the RWPs. However, that study focused on the northern hemisphere, and did not distinguish between short and long-lived RWPs. Recent studies have characterized RWPs in the southern hemisphere and show that in the summer LLRWPs represent about 10% of the total RWPs and their frequency of occurrence is influenced by the Southern Annular Mode (SAM) and El Niño-Southern Oscillation (ENSO) (Pérez et al., 2021; Sagarra & Barreiro, 2020). As a continuation of these studies, here we aim to analyze whether S2S models are able to forecast the development and trajectories of LLRWPs. To do so, we compare the trajectories of LLRWPs tracked in a reanalysis against the trajectories of the LLRWPs forecasted by two S2S models. Additionally, we studied whether LLRWPs forecast is affected by the area where the LLRWPs first manifested, the dominant SAM or ENSO phase, or by the Madden Julian Oscillation (MJO).

The paper is organized as follows. Section 2 describes the datasets, the RWPs tracking methodology and the analysis performed to assess LLRWPs representation in both models. Section 3 shows the results followed by a discussion and Section 4 presents a summary of the study.

2 | DATA AND METHODOLOGY

2.1 | Data

In this study we used the ERA 5 Reanalysis (Hans et al., 2020), with an horizontal resolution of $0.25 \times 0.25^\circ$,

and two S2S models: the NCEP CFSV2 (Saha et al., 2014), hereafter NCEP, and the CAS FGOALS f2 V1.3, hereafter IAP-CAS (Bao et al., 2019; Bao & Li, 2020; He et al., 2019; Li et al., 2019). The NCEP (IAP-CAS) model has a spatial resolution of $1.5 \times 1.5^\circ$ ($1 \times 1^\circ$) and a forecast length of 45 (65) days. Both models have daily reforecast data and 4-members ensemble simulations (1 control and 3 perturbed). Datasets were regridded to a spatial resolution of 2.5° , and the length of the forecast was limited to 45 days.

The period of study focuses in the southern hemisphere summer (December to March, or DJFM) as done in Sagarra and Barreiro (2020) and Pérez et al. (2021). We restricted our analysis to the DJFM season between 1999 and 2010, due to time constraints of the NCEP dataset, having 11 DJFM seasons available for the analysis.

RWPs propagate in the atmosphere as meanders of the jet stream, producing a series of troughs and ridges restricted to a certain latitudinal band and showing a mainly eastward direction during austral summer (Chang, 1999b). Therefore, RWPs can be characterized by computing the envelope that surrounds the packet. In order to compute the envelope (V_{300env} , in m/s) we used meridional winds at 300 hPa (V_{300}) following the methodology detailed in Pérez et al. (2021). Given that RWPs propagation is mainly zonal during southern hemisphere summer (Chang, 1999a, 1999b), we average the data in the latitudinal band between 40 and 65° S.

2.2 | Description of RWPs tracking algorithm and detection of LLRWPs

Prior to the application of the RWPs tracking algorithm, we need to filter out low amplitude V_{300env} data to avoid tracking noise. Nevertheless, the selection of the threshold is not obvious because there are no physical properties that separate one packet from another (Souders et al., 2014b). We apply a threshold of 19 m/s (Pérez et al., 2021) for ERA 5, and a threshold of 18 (17) m/s for NCEP (IAP-CAS) data. The chosen thresholds are based on the distribution of 7-day running mean values of V_{300env} , shown in Figure S1 (as done in Grazzini & Vitart, 2015; and Sagarra & Barreiro, 2020). The method considers that V_{300env} values smaller than the median of the distribution are noise and thus are set to zero.

The tracking algorithm is based on the maximum envelope technique (Grazzini & Vitart, 2015; Pérez et al., 2021; Sagarra & Barreiro, 2020), which locates areas with the maximum daily values of V_{300env} above a

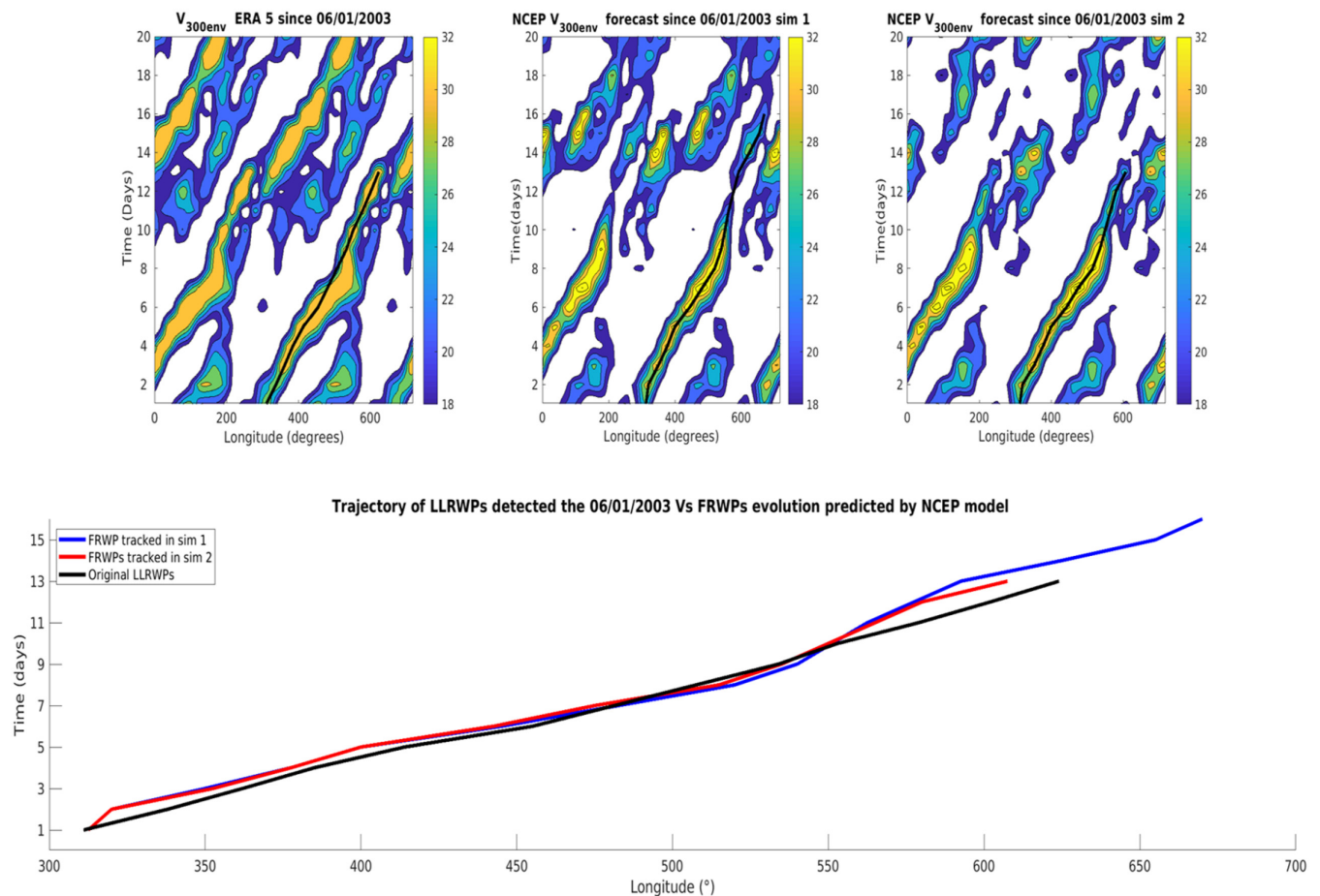


FIGURE 1 Hovmoller diagram of V_{300env} (in m/s) during the propagation of a LLRWPs detected in the reanalysis at 06/01/2003 (upper left), NCEP V_{300env} forecast from the first 2 perturbed simulations (upper mid and upper right), plus graphical representation of the tracked trajectories (down figure). Black lines in the upper figures identify the trajectory of the original LLRWPs (FRWPs) detected in the reanalysis (forecast), and colored lines in the down figure identify the trajectories of the observed LLRWPs and FRWPs.

minimum threshold, identifying the RWPs center of activity, and then follows their propagation to the east assuming that the packets travel with speeds between 15 and 45°/day. After the tracking stage, the algorithm links truncated trajectories using proximity criteria and registers the RWPs characteristics. Afterwards, we retained RWPs that lasted more than 8 days (LLRWPs) and registered the dates when the LLRWPs are detected (T_d) and their areas of formation (X_d). A full detailed description of the algorithm is available in Pérez et al. (2021). Finally, it is important to highlight that this algorithm requires a zonally symmetric wind flow (Grazzini & Vitart, 2015), which is only observed during austral summer (Chang, 2000).

To search for LLRWPs in the S2S models, we downloaded the reforecast datasets starting the forecasts at days T_d , and transformed V_{300} into V_{300env} following the methodology mentioned in Section 2.1. The tracking algorithm is then applied to each simulation to search for forecasted LLRWPs. As we search

for RWPs that starts close to X_d , before the tracking stage, V_{300env} forecast outside the range $[X_d - R + V_{min} \times (T_n - 1), X_d + R + V_{max} \times (T_n - 1)]$ for lead days 1–3 of simulation is deleted from the datamatrix. R is a typical Rossby radius (1000 km), T_n the lead day of the forecast and V_{min} (V_{max}) the minimum (maximum) propagation speed of the packets, here considered as 10 (50)°/day to allow for small biases in the reforecasted data.

After the tracking stage, we search in every simulation for LLRWPs that start their propagation between lead days 1–3 of the forecast. If the tracking algorithm detects a LLRWP that matches this condition, we save that trajectory as the forecasted evolution of a LLRWP (hereafter FRWP), else, we assume that the simulation failed to predict a FRWPs and proceed to the next simulation. An example for the NCEP model is displayed in Figure 1, where a LLRWP was detected in ERA 5, and two NCEP simulations where FRWPs are close to the observed LLRWP.

2.3 | Representation of LLRWPs in the forecast models, and the influence of SAM, ENSO and MJO

We start by analyzing whether the forecast models can predict the development of the LLRWPs. To do so, first we measured the proportion of ensemble members able to predict a FRWPs/FRWPs that lasted more than 8 days during different ENSO/SAM phases. The classification of the SAM and ENSO phases follows the same criteria as in Pérez et al. (2021).

Second, in order to study how similar are the FRWPs compared to the observed LLRWPs, we measured the zonal displacement between the observed LLRWPs trajectory and the FRWPs the first 9 days after the detection of the observed LLRWPs. Additionally, in order to infer how energetic are the FRWPs compared to the observed LLRWPs, we studied the differences between the $V_{300\text{env}}$ at the center of the observed LLRWPs against the forecasted values of $V_{300\text{env}}$ found at the center of the FRWPs.

Third, we classified simulations as best/good/bad/worst forecasts as those that were able to predict the development of a LLRWPs in (100–75)/50/25/0% of the ensemble members, respectively. It is worth pointing out that results of model performance may change by using a larger ensemble.

Fourth, we examined whether LLRWPs forecast is affected by the area where LLRWPs are first detected. To assess this we considered six zonal bands: 0–60° E, 61–120° E, 121–180° E, 181–240° E, 241–300° E, 301–359° E.

Next, we measured the differences in geopotential height anomaly at 300 hPa (Z_{a300}) using reanalysis and reforecast data during the best/worst LLRWPs forecasts. This is to assess the differences in the mean atmospheric circulation. In order to do so, we constructed the mean Z_{a300} from days $T_d - T_{d+10}$, being T_d the starting dates of simulations with the best/worst LLRWPs forecasts. Afterwards, we assess the statistical significance of the results using a Student *t*-test at 10% level, comparing Z_{a300} data that belong to dates with best/worst forecasts of LLRWPs against the rest of the dataset (Z_{a300} data that do not belong to best/worst forecasts).

Lastly, we studied MJO activity during the periods with the best/worst LLRWPs forecasts to assess whether the propagation of MJO during the LLRWPs lifetime affects the LLRWPs forecast. To do so, we first calculated the climatological frequency of having the MJO in every stage (C), and its standard deviation (STD) during austral summer between 1979 and 2020. Next, we calculated the probability of finding every MJO phase during the first 10 days since day T_d for the best/worst LLRWPs forecasts. If the relative frequency of occurrence of a certain

MJO phase during good/bad forecasts is outside the range $C \pm \text{STD}$, that MJO stage is more frequent/absent than usual.

3 | RESULTS AND DISCUSSION

3.1 | LLRWPs tracking, ENSO and SAM influence

We found 39 LLRWPs in the austral summer between 1999 and 2010 (around 3.5 LLRWPs per season), 20 LLRWPs were found during neutral SAM years, 14 in negative SAM and 5 in positive SAM years. In the case of ENSO events, 15 LLRWPs appear in La Niña events, 8 for Neutral ENSO and 16 in El Niño years. These results are consistent with Pérez et al. (2021) and with the fact that during positive SAM the strengthening of the westerlies diminishes the meandering of the flow.

As each model has four simulations available, there are 156 simulations available per model. The NCEP model was able to forecast the formation of FRWPs in 86% of the simulations, and 52% of them surpassed the 8 days threshold. FRWPs showed a mean lifespan of 9.1 ± 4.7 days. The IAP-CAS forecasted the development of FRWPs in 84% of the simulations, although barely 40% of them lasted more than 8 days. FRWPs tracked last around 8.2 ± 4.4 days. Oppositely, observed LLRWPs displayed a mean lifespan of 13.0 ± 2.7 days. Therefore, forecast models can predict LLRWPs development but underestimate their lifespan. A distribution of observed LLRWPs and FRWPs lifetime is shown in Figure S2.

Table 1 shows the proportion of total FRWPs/FRWPs that lasted more than 8 days that were correctly forecasted by the models during different SAM/ENSO events. In the NCEP model, the proportion of FRWPs found during years with positive SAM is lower compared to other SAM phases, and neutral ENSO shows the largest proportion of detected FRWPs. Overall, in the IAP-CAS model we have similar results to those observed in NCEP. Nonetheless, for FRWPs that surpassed the 8 day threshold, the highest (lowest) proportion is found during positive SAM events in the NCEP (IAP-CAS) model. This large difference between models might be due to the low number of cases during positive SAM events, which makes the results very sensitive to small differences. Meanwhile, for ENSO events the NCEP model shows the highest (lowest) proportion of FRWPs that surpassed the 8 days threshold in La Niña (neutral) years. In contrast, for the IAP-CAS model, the highest (lowest) proportion of FRWPs with lifespan above 8 days is detected in neutral (La Niña) years.

TABLE 1 Proportion of total FRWPs and FRWPs that lasted more than 8 days found in forecasts during different SAM and ENSO stages in NCEP and IAP-CAS model.

Total FRWPs detection (%)	El Niño	Neutral	La Niña	SAM+	SAM neutral	SAM–
NCEP	85	97	78	70	89	85
IAP-CAS	87	84	76	75	87	79
Frequency of FRWPs that lasted more than 8 days in the simulation/ total FRWPs detection (%)						
NCEP	51	38	59	64	38	59
IAP-CAS	41	59	28	20	46	39

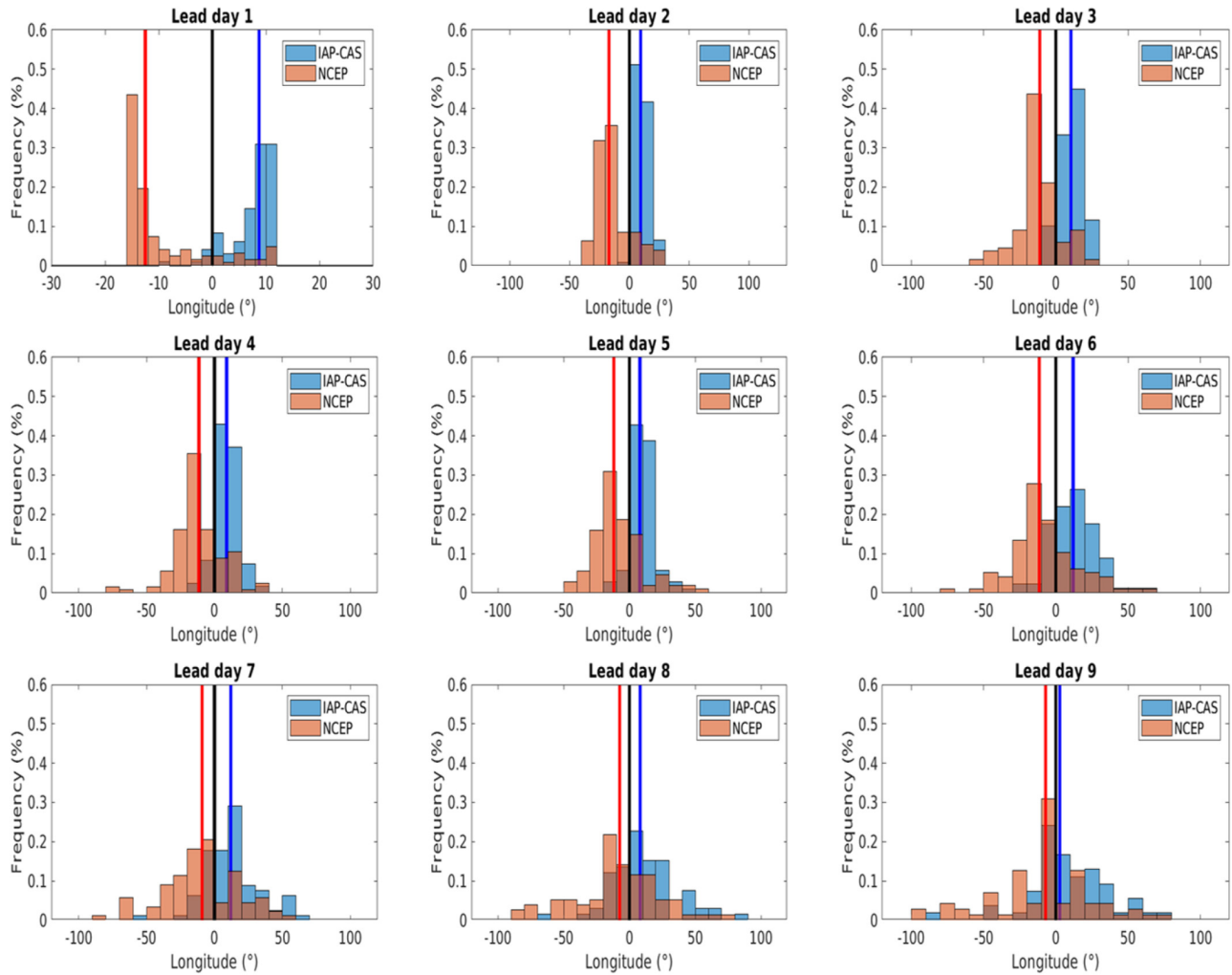


FIGURE 2 Frequency histogram of the FRWPs displacement from the original LLRWPs found in the reanalysis in each lead day. Positive (negative) bias signals that the FRWPs appear more westwards (eastwards) compared to the observed LLRWPs. Black lines signals the area of 0 bias whereas red (blue) lines show the median location of the FRWPs tracked in the ensemble mean for NCEP (IAP-CAS) forecast.

We generally find lower frequencies of FRWPs that lasted more than 8 days in IAP-CAS. This is consistent with the fact that FRWPs detected by the NCEP model have longer lifespans compared to those found in IAP-CAS.

3.2 | Model representation of LLRWPs and influence of the MJO

Figure 2 shows the zonal displacement between the location of the observed LLRWPs and the FRWPs the first

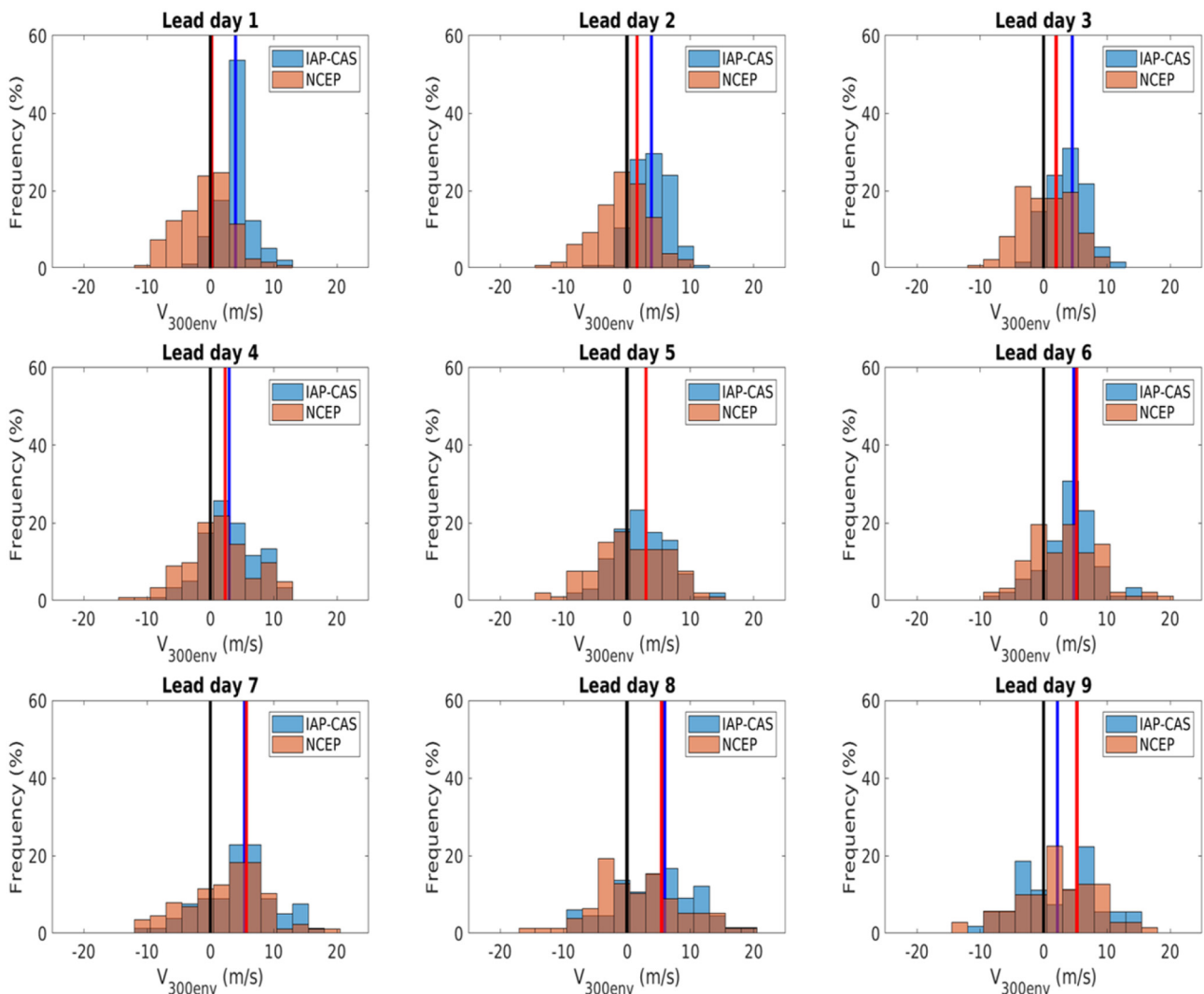


FIGURE 3 Analogous to Figure 2, but for $V_{300\text{env}}$ differences at the center of the wave packet on the observed LLRWPs against its forecasted trajectory. Positive (negative) values signal that the FRWPs have lower (higher) $V_{300\text{env}}$, thus, RWPs forecasted by the model are less (more) energetic compared to the observed LLRWPs.

9 days of the packets lifespan. FRWPs detected in the NCEP (IAP-CAS) model tend to appear more to the east (west) from the observed packet. This pattern remains approximately constant after day one until the 8–9th lead day, when the median of both distributions is near zero. This change could be attributed to the loss of FRWPs as the simulation advances.

In Figure 3, we display the difference of $V_{300\text{env}}$ at the center of the packet between the observed LLRWPs minus the tracked FRWPs in each lead day of simulation. Positive (negative) values signal that the forecast model underestimates (overestimates) the energy contained within the packet. Initially, the NCEP model does not greatly differ from the reanalysis. Nonetheless, starting on the 6th lead day of the simulation, the energy contained in FRWPs decays rapidly, indicating that FRWPs are less energetic compared to

the observed LLRWPs. Nevertheless, wave packets tracked in the IAP-CAS always tend to underestimate the energy contained in the observed wave packets. Thus, even though both models detect a similar number of FRWPs, IAP-CAS is much less energetic compared to the reanalysis.

Giannakaki and Martius (2016) showed that forecast models in the northern hemisphere usually underestimate the area and strength of the waveguide. Moreover, Gray et al. (2014) concluded that in the northern hemisphere, the potential vorticity fields where RWPs propagate fall rapidly with lead time in numerical weather prediction models. Therefore, an underestimation of the potential vorticity anomaly fields as the forecast advances, causes that $V_{300\text{env}}$ in the forecast diminishes faster than in the reanalysis. It is plausible to think that a similar process can be at work in the southern

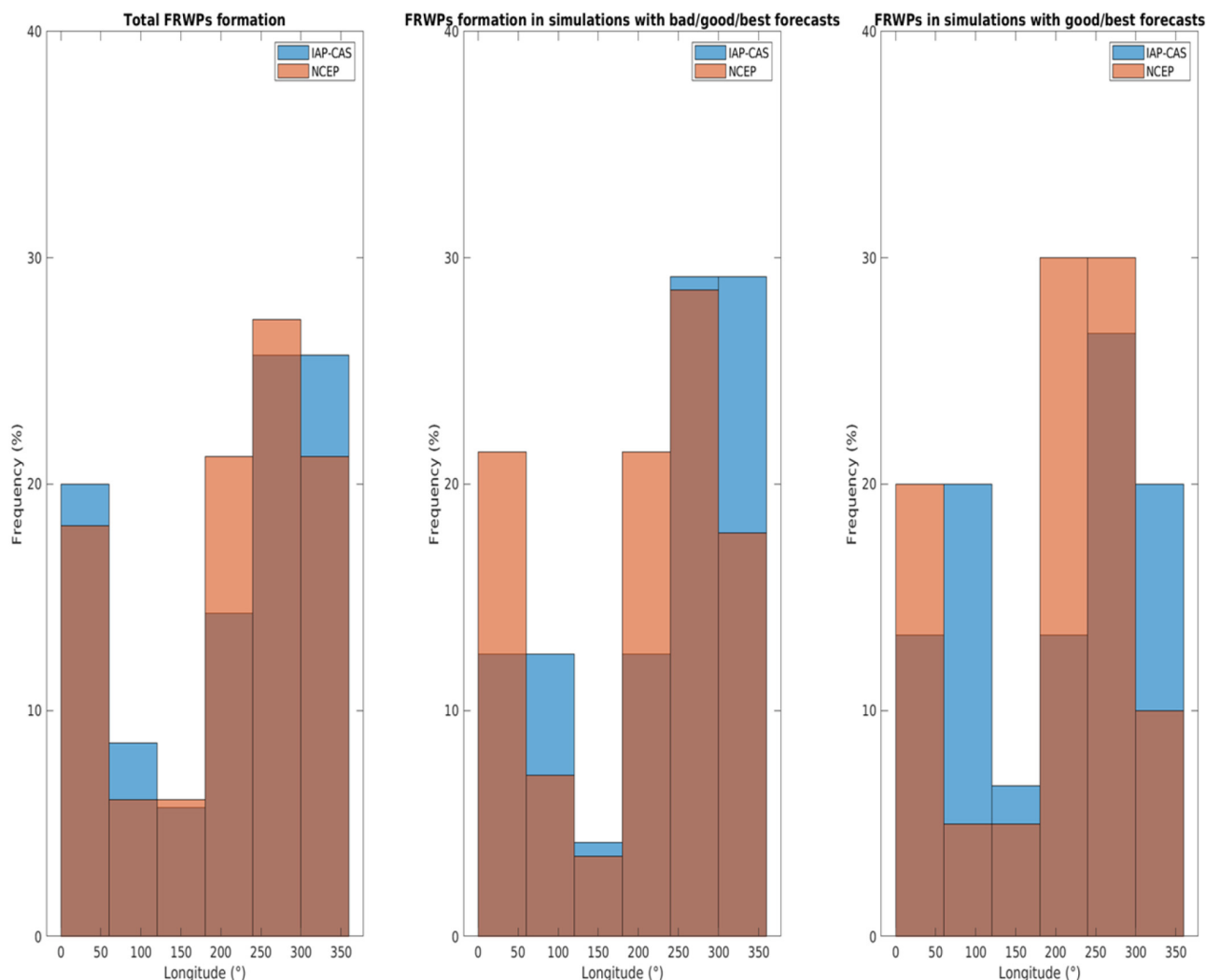


FIGURE 4 Detection areas of total FRWPs/proportion FRWPs that lasted more than 8 days in the simulations.

hemisphere, therefore, LLRWPs forecasts might be limited to the synoptic scale.

When we focus on the classification of the simulations, near 18% of the NCEP simulations belong to the worst forecasts, 23% to bad forecasts, and 59% to good or the best forecasts. Conversely, 36% of the IAP-CAS simulations belong to the worst forecasts, 26% to bad forecasts, whereas only 38% belong to the good/best forecasts. These results further suggest that the NCEP model is better at forecasting LLRWPs compared to the IAP-CAS. Figure 4 shows the areas where the total proportion of FRWPs/FRWPs with lifespan above 8 days. Both models show that most of FRWPs were first detected in the eastern Pacific (241–300° E), and western South-Atlantic basins (301–359° E). But when we retain simulations that are part of good and/or best forecasts, most of FRWPs were first detected at the central-eastern Pacific basin (180–300° E) in the NCEP model, and in the eastern Pacific (241–300° E) for the IAP-CAS model. One

possibility that might explain these results is that the eastern Pacific basin has a maximum of baroclinity (Solman et al., 2003), which favor RWPs development. Thus, RWPs that appear in the eastern Pacific basin will propagate toward the Atlantic-Indian sector where the jet stream, which acts as a waveguide where RWPs propagate, reaches its maximum intensity. Consequently, FRWPs gain stability and propagate for longer periods.

We next examine the mean atmospheric flow in the reanalysis and forecast models during the best/worst forecasts (Figure 5). It is worth mentioning that Pérez et al. (2021) concluded that the northward displacement of the jet stream (this is, during negative SAM events) causes the development of a cyclonic circulation to the southwest of New Zealand. This enables the extension of the waveguide where RWPs propagate into the Pacific, thus favoring LLRWPs. In agreement with this study, Figure 5 shows in all panels an anomalous cyclonic circulation to the southwest of New Zealand. Moreover, this

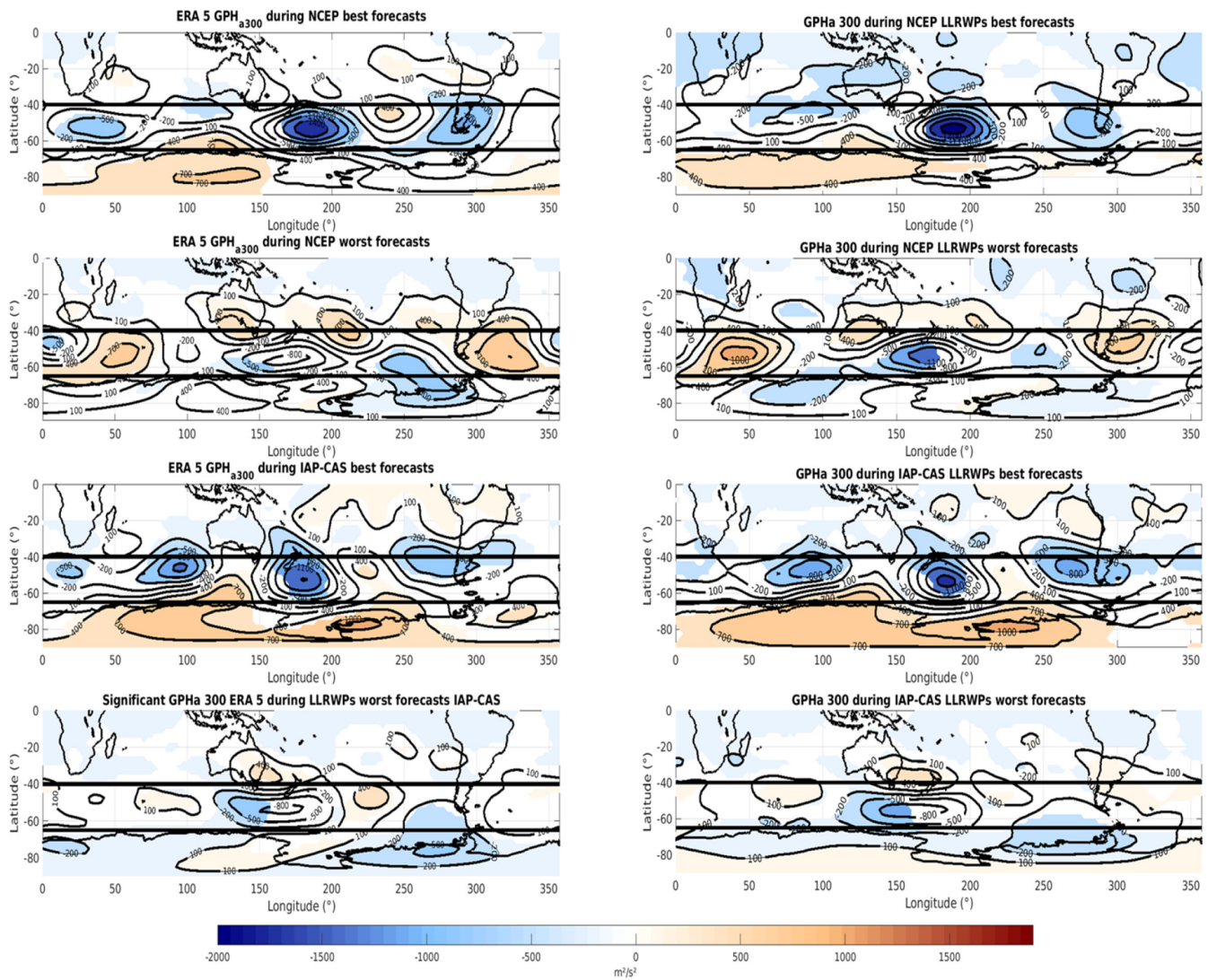


FIGURE 5 Z_{a300} fields from $T_d - T_{d+10}$, being T_d the dates when we obtained the best/worst forecast skill in the NCEP and IAP-CAS models. Left (right) figures show the Z_{a300} field obtained using the reanalysis (forecast) data. Orange (blue) areas signal positive (negative) anomalies.

cyclonic circulation is strongest and is accompanied by generally low geopotential height anomalies between 40° S and 60° S during the best forecasts. In addition, Z_{a300} in high latitudes significantly increases during the best forecasts which, together with the negative Z_{a300} in midlatitudes signal the manifestation of negative SAM events. Consequently, results suggest that LLRWPs forecasting might be more feasible during negative SAM years. Alternatively, during the worst forecasts, the circulation anomalies do not show a clear common global pattern. There seems to exist a stationary wave extending from Australia southwards in both models. However, in NCEP forecasts, there are several positive Z_{a300} anomalies in subtropical latitudes, that are not present in IAP-CAS. These findings suggest that some atmospheric processes might lead to the development of a stationary wave near

New Zealand which impedes RWPs propagation into the Pacific. Furthermore, the spatial structure suggests that the wave patterns of Figure 5 may be at least partly forced from the tropical region. To further look into that we explore the possibility that the MJO may play a role.

Figure 6 shows the probability of occurrence of a certain MJO phase during the best/worst forecasts against their climatological frequency. During the best forecasts, both models show an anomalously inactive MJO, and phases 4–8 are specially absent, particularly in the IAP-CAS model. Also, the probability of finding phases 1–3 is near climatology. By contrast, during the worst forecasts in the NCEP model, the MJO is more active than usual in phases 3 and 5, oppositely, phases 1–2 are mostly absent, whereas the remaining phases occur near climatology. In the IAP-CAS model, the worst

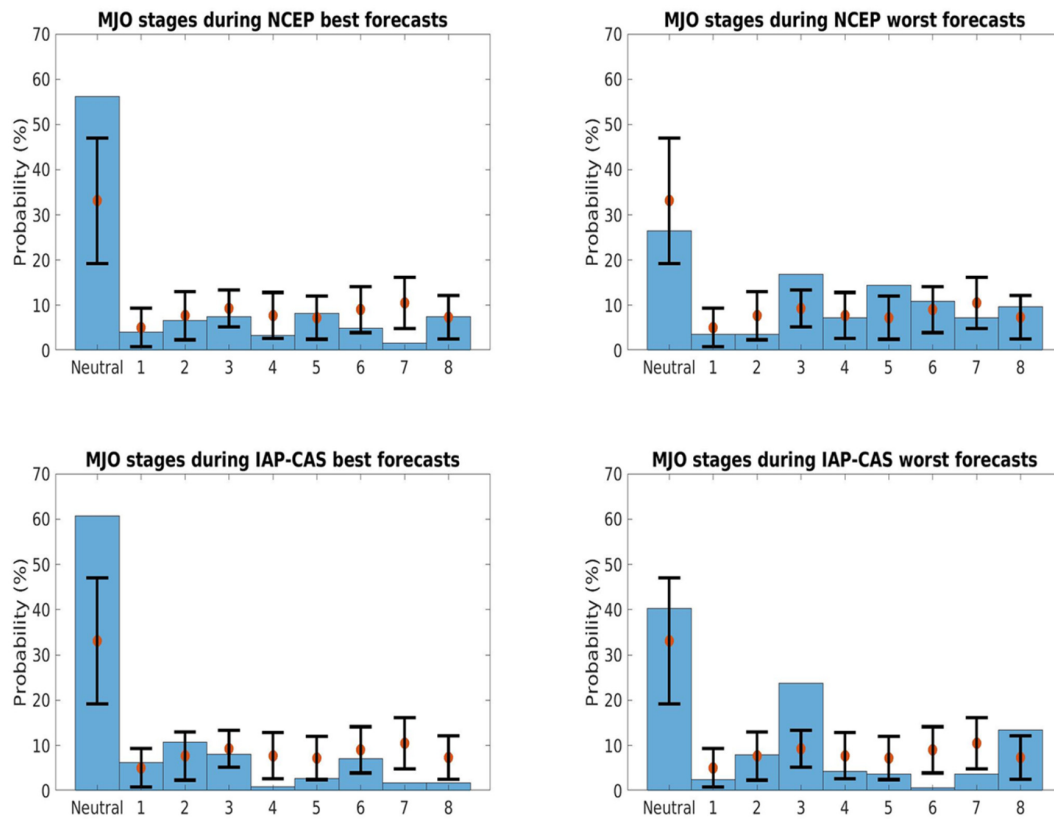


FIGURE 6 Relative frequency of the MJO phases detected during the propagation of LLRWPs for the best (left figures) and worst (right figures) forecasts found in NCEP and IAP-CAS models. Orange dots represent the mean climatological probability of finding the MJO in a specific phase whereas back lines show the range between mean climatological probability \pm its standard deviation.

forecasts are also characterized by an active MJO, particularly in phases 3 and 8, appearing with much higher frequency than the climatology. Thus, in both models the best (worst) forecasts are characterized by an inactive (active) MJO.

The Z_{a300} patterns shown in the composite of the worst forecasts of the NCEP and IAP-CAS models (Figure 5), do not match with circulation anomalies associated with their most frequent stages of the MJO (see Figure 1 of Alvarez et al., 2016). One reason that might explain these results is that because the MJO is more active than usual in certain phases, the anomalies observed are a mixture of signals without a defined structure. Therefore, the maps obtained are not similar between models, and usually show weaker Z_{a300} values that are less significant than the anomalies associated with the best forecasts.

Results show that an active MJO degrades the LLRWPs forecast, which might be attributed to the interaction between the tropically excited and mid-latitude waves. Nonetheless, we have to take into consideration that even though the MJO forecast is reliable until 25 days in advance (Fu et al., 2013), current biases in the representation of the MJO and its teleconnections (Lim et al., 2018) may degrade LLRWP predictions.

4 | CONCLUSIONS

RWPs are considered precursors of extreme weather events. Under certain circumstances they can last for several days to weeks in the atmosphere, thus, studying the representation of these long-lived packets might improve extreme weather event detection in the sub-seasonal time scale. Here we considered two S2S models (NCEP and IAP-CAS), and showed that they are capable of forecasting long-lived RWPs. Nevertheless, packets forecasted by NCEP (IAP-CAS) model are systematically shifted to the east (west) from the original packet, although they propagate with similar speeds. Both NCEP and IAP-CAS models struggle to forecast RWPs that last more than a week because predicted packets rapidly lose energy after the first week of simulation, which might limit long-lived RWPs forecast to the synoptic scale. Both models accurately represent long-lived RWPs that appear in the eastern Pacific sector, and also during negative SAM events. However, the worst forecasts of both models manifest a stationary wave train that blocks the propagation of wave packets to the south of Australia. Moreover, MJO influences LLRWPs forecast in the models, such that during simulations with

good LLRWPs forecasts the MJO is anomalously inactive in both models. In contrast, during the worst LLRWPs forecasts, some MJO phases are more active than usual (phases 3, 5 in the NCEP model and 3, 8 for IAP-CAS) and results show a mixture of signals with lower significance and amplitude that do not seem to be linked to a specific MJO phase. These differences between models may be due to distinct simulated MJO dynamics and teleconnections, or could be related to the misrepresentation of the MJO in the forecast, complicating the identification of MJO phases that might favor LLRWPs forecast. Nevertheless, our results suggest that LLRWPs prediction in two sub-seasonal models is influenced by the activity of the MJO, and inactive (active) periods of MJO lead to improve (degrade) LLRWPs forecasts. Future studies should focus on determining whether the misrepresentation of the MJO in forecasts models greatly affects RWP predictions in the mid-latitudes of the southern hemisphere.

AUTHOR CONTRIBUTIONS

Iago Perez Fernandez: Data curation; formal analysis; investigation; methodology; resources; software; validation; visualization; writing – original draft. **Marcelo Barreiro:** Conceptualization; formal analysis; funding acquisition; investigation; methodology; project administration; supervision; visualization; writing – review and editing.

ACKNOWLEDGMENTS


This project has received funding from the European Union's Horizon 2020 research and innovation programme under the Marie Skłodowska-Curie grant agreement No. 813844 (ITN CAFÉ). We also acknowledge support by Programa de Desarrollo de las Ciencias Básicas (PEDECIBA).

DATA AVAILABILITY STATEMENT

ERA5 reanalysis data is freely available in the Copernicus Climate Data Store <https://cds.climate.copernicus.eu/>, and the envelope of the RWP used in this study can be downloaded at <https://doi.org/10.5281/zenodo.5714192>, as well as a script to measure wind envelope data from meridional wind speed at <https://doi.org/10.5281/zenodo.5724656>. NCEP CFSv2 and IAP-CAS reforecast datasets can be downloaded at the IRI/LDEO Biblioteca de Datos Climáticos and ECMWF S2S database in the links: <https://iridl.ldeo.columbia.edu/SOURCES/.ECMWF/.S2S/.NCEP/> and <https://apps.ecmwf.int/datasets/data/s2s/levtype=sfc/type=cf/>, respectively. MJO index data was downloaded from the Bureau of meteorology website: <http://www.bom.gov.au> and ENSO and SAM indexes can be downloaded at <https://origin.cpc.ncep.noaa.gov/>.

ORCID

Iago Pérez-Fernández  <https://orcid.org/0000-0003-2575-9470>

Marcelo Barreiro  <https://orcid.org/0000-0002-7819-1607>

REFERENCES

- Alvarez, M.S., Vera, C.S., Kiladis, G.N. & Liebmann, B. (2016) Influence of the Madden Julian Oscillation on precipitation and surface air temperature in South America. *Climate Dynamics*, 46, 245–262. Available from: <https://doi.org/10.1007/s00382-015-2581-6>
- Bao, Q. & Li, J. (2020) Progress in climate modeling of precipitation over the Tibetan plateau. *National Science Review*, 7(3), 486–487. Available from: <https://doi.org/10.1093/nsr/nwaa006>
- Bao, Q., Wu, X.F., Li, J.X., Wang, L., He, B., Wang, X.C. et al. (2019) Outlook for El Niño and the Indian Ocean dipole in Autumn-winter 2018–2019. *Chinese Science Bulletin*, 64(1), 73–78. Available from: <https://doi.org/10.1360/N972018-00913>
- Chang, E.K.M. (1999b) Characteristics of wave packets in the upper troposphere. Part II: Seasonal and hemispheric variations. *Journal of Atmospheric Sciences*, 56(11), 1729–1747. Available from: [https://doi.org/10.1175/1520-0469\(1999\)056<1729:COWPIT>2.0.CO;2](https://doi.org/10.1175/1520-0469(1999)056<1729:COWPIT>2.0.CO;2)
- Chang, E.K.M. & D.B. Yu. (1999a) Characteristics of wave packets in the upper troposphere. Part I: Northern Hemisphere winter. *Journal of Atmospheric Sciences*. 56(11), 1708–1728.
- Chang, E.K.M. (2000) Wave packets and life cycles of troughs in the upper troposphere: examples from the southern hemisphere, summer season of 1984/1985. *Monthly Weather Review*, 128(1), 25–50. Available from: [https://doi.org/10.1175/1520-0493\(2000\)128<0025:WPALCO>2.0.CO;2](https://doi.org/10.1175/1520-0493(2000)128<0025:WPALCO>2.0.CO;2)
- Chang, E.K.M. (2005) The impact of wave packets propagating across Asia on Pacific cyclone development. *Monthly Weather Review*, 133, 1998–2015. Available from: <https://doi.org/10.1175/MWR2953.1>
- Chang, E.K.M. & Yu, D.B. (1999) Characteristics of wave packets in the upper troposphere. Part I: Northern Hemisphere winter. *Journal of Atmospheric Sciences*, 56(11), 1708–1728. Available from: [https://doi.org/10.1175/1520-0469\(1999\)056<1708:COWPIT>2.0.CO;2](https://doi.org/10.1175/1520-0469(1999)056<1708:COWPIT>2.0.CO;2)
- Fu, X.H., Lee, J.Y., Hsu, P.C., Taniguchi, H., Wang, B., Wang, W.Q. et al. (2013) Multi-model MJO forecasting during DYNAMO/CINDY period. *Climate Dynamics*, 41, 1067–1081. Available from: <https://doi.org/10.1007/s00382-013-1859-9>
- Giannakaki, P. & Martius, O. (2016) An object-based forecast verification tool for synoptic-scale Rossby waveguides. *Weather and Forecasting*, 31(3), 937–946. Available from: <https://doi.org/10.7892/boris.83861>
- Gray, S.L., Dunning, M.C., Methven, J., Masato, G. & Chagnon, M. J. (2014) Systematic model forecast error in Rossby wave structure. *Geophysical Research Letters*, 41, 2979–2987. Available from: <https://doi.org/10.1002/2014GL059282>
- Grazzini, F. & Vitart, F. (2015) Atmospheric predictability and Rossby wave packets. *International Journal of the Royal Meteorological Society*, 141(692), 2793–2802. Available from: <https://doi.org/10.1002/qj.2564>
- Hans, H., Bell, B., Berrisford, P., Hirahara, S., Horány, A., Muñoz-Sabater, J. et al. (2020) The ERA5 global reanalysis. *Quarterly*

- Journal of Royal Meteorological Society*, 146(730), 1999–2049. Available from: <https://doi.org/10.1002/qj.3803>
- He, B., Bao, Q., Wang, X., Zhou, L., Wu, X., Liu, Y. et al. (2019) CAS FGOALS-f3-L model datasets for CMIP6 historical atmospheric model intercomparison project simulation. *Advances in Atmospheric Sciences*, 36(8), 771–778. Available from: <https://doi.org/10.1007/s00376-019-9027-8>
- Li, J., Bao, Q., Liu, Y., Wu, G., Wang, L., He, B. et al. (2019) Evaluation of FAMIL2 in simulating the climatology and seasonal-to-interannual variability of tropical cyclone characteristics. *Journal of Advances in Modeling Earth Systems*, 11(4), 1117–1136. Available from: <https://doi.org/10.1029/2018MS001506>
- Lim, Y., Son, S.W. & Kim, D. (2018) MJO prediction skill of the subseasonal-to seasonal prediction models. *Journal of Climate*, 31(10), 4075–4094. Available from: <https://doi.org/10.1175/JCLI-D-17-0545.1>
- O'Brien, L. & Reeder, J.M. (2017) Southern hemisphere summertime Rossby waves and weather in the Australian region. *Quarterly Journal of the Royal Meteorological Society*, 143(707), 2374–2388. Available from: <https://doi.org/10.1002/qj.3090>
- Pérez, I., Barreiro, M. & Masoller, C. (2021) ENSO and SAM influence on the generation of long episodes of Rossby wave packets during southern hemisphere summer. *Journal of Geophysical Research: Atmospheres*, 126, e2021JD035467. Available from: <https://doi.org/10.1029/2021JD035467>
- Quinting, J.F. & Vitart, F. (2019) Representation of synoptic-scale Rossby wave packets and blocking in the S2S prediction project database. *Geophysical Research Letters*, 46, 1070–1078. Available from: <https://doi.org/10.1029/2018GL081381>
- Sagarra, R. & Barreiro, M. (2020) Characterization of extratropical waves during summer of the southern hemisphere. *Meteorologica*, 45, 63–79.
- Saha, S., Moorthi, S., Wu, X., Wang, J., Nadiga, S., Tripp, P. et al. (2014) The NCEP climate forecast system version 2. *Journal of Climate*, 27(6), 2185–2208. Available from: <https://doi.org/10.1175/JCLI-D-12-00823.1>
- Solman, S.A., Núñez, M.N. & Rowntree, P.R. (2003) On the evaluation of the representation of mid-latitude transients in the southern hemisphere by HadAM2B GCM and the impact of horizontal resolution. *Atmosfera*, 16(4), 257–283.
- Souders, B.M., Colle, A.B. & Chang, M.K.D. (2014a) The climatology and characteristics of Rossby wave packets using a feature-based tracking technique. *Monthly Weather Review*, 142(10), 3528–3548. Available from: <https://doi.org/10.1175/MWR-D-13-00371.1>
- Souders, B.M., Colle, A.B. & Chang, M.K.D. (2014b) A description and evaluation of an automated approach for feature-based tracking of Rossby wave packets. *Monthly Weather Review*, 142(10), 3505–3527. Available from: <https://doi.org/10.1175/MWR-D-13-00317.1>
- Wirth, V., Riemer, M., Chang, E.K.M. & Martius, O. (2018) Rossby wave packets on the midlatitude waveguide—a review. *Monthly Weather Review*, 146(7), 1965–2001. Available from: <https://doi.org/10.1175/MWR-D-16-0483.1>
- Yeh, T.C. (1949) On energy dispersion in the atmosphere. *Journal of Meteorology*, 6(1), 1–16. Available from: [https://doi.org/10.1175/1520-0469\(1949\)006<0001:OEDITA>2.0.CO](https://doi.org/10.1175/1520-0469(1949)006<0001:OEDITA>2.0.CO)
- Zheng, M., Chang, E.K. & Colle, B.A. (2013) Ensemble sensitivity tools for assessing extratropical cyclone intensity and track predictability. *Weather and Forecasting*, 28(5), 1133–1156. Available from: <https://doi.org/10.1175/WAF-D-12-00132.1>

SUPPORTING INFORMATION

Additional supporting information can be found online in the Supporting Information section at the end of this article.

How to cite this article: Pérez-Fernández, I., & Barreiro, M. (2023). How well do forecast models represent observed long-lived Rossby wave packets during southern hemisphere summer? *Atmospheric Science Letters*, 24(10), e1175. <https://doi.org/10.1002/asl.1175>